Supplementary information for

Enhancing Energy-Storage Characteristics of BNT-Based Ceramic via Quadruple Perovskite ($AA'_3B_4O_{12}$) Modification

Amiya Mandal, Deepanshu Kaneria, Shivam Kumar Mittal, Munendra Pal, Kanhaiya Lal Yadav*

Smart Material Research Laboratory, Department of Physics, Indian Institute of Technology Roorkee, Roorkee. India, 247667

***Corresponding author**

E-mail address: klyadav35@gmail.com

Experimental Details

• Synthesis

The (1−x)$Bi_{0.47}Na_{0.47}Ba_{0.06}TiO_3$–x$CaCu_3Ti_4O_{12}$ powders, abbreviated as (1−x)BNBT–xCCTO with x = 0, 0.02, 0.04, 0.06 and 0.08, were prepared using a standard solid-state ceramic route. Commercial oxide and carbonate powders of high purity (Bi_2O_3 >99.9%, Na_2CO_3 >99.8%, TiO_2 99%, $CaCO_3$ 99%, CuO 99% and $BaCO_3$ 99%; Hi-Media, India) served as the precursors. The weighed chemicals were first mixed in ethanol and ball-milled for 24 h at 300 rpm using zirconia media, which helped to distribute the components evenly. After removing the solvent, the mixed powder was heat-treated at 850 °C for 4 h to initiate the reaction.

The calcined material was then milled again to break up soft agglomerates and improve powder flow. A small amount of PVA solution was added so that the powder could be shaped into discs approximately 12 mm in diameter and 1 mm thick under a uniaxial pressure of 350 MPa. The binder was burned out by heating the compacts to 600 °C for about 30 min, and final densification took place at 1150 °C for 2 h. To minimise the volatilisation of Bi^{3+} and Na^+ during high-temperature sintering, the pellets were sintered in covered alumina crucibles under controlled conditions.

• Characterization Methods

Phase formation and crystal structure were examined using a Rigaku SmartLab X-ray diffractometer equipped with Cu-K_α radiation (λ = 1.5406 Å). Diffraction patterns were collected over 20–80° in 2θ with a step size of 0.02°. Room-temperature Raman spectra were recorded directly from polished pellets using a Nanoscope Raman spectrometer fitted with a 633.40 nm He–Ne laser. Microstructural observations were performed on fracture surfaces using a field-emission scanning electron microscope (FE-SEM; Zeiss Ultra Plus, Carl Zeiss, Germany). In addition, a Talos F200X (S)TEM (Thermo Fisher Scientific) was employed to visualise domain morphology, acquire high-resolution TEM images, and perform SAED analysis. For nanoscale domain mapping, piezoresponse force microscopy (PFM) was conducted on a Bruker Dimension ICON AFM system.

Temperature- and frequency-dependent dielectric measurements were obtained using a HIOKI 3532-50 LCR meter, which also enabled electrochemical impedance spectroscopy (EIS) analysis. Prior to electrical testing, pellets with silver electrodes were dried at 200 °C for approximately 45 min to ensure stable contact. For energy-storage measurements, sintered disks were thinned to 0.10–0.20 mm and coated with circular electrodes of 2 mm diameter on both faces. Polarisation–electric field (P–E) loops were collected on a commercial ferroelectric test system (Marine India) operated in silicone oil to prevent dielectric breakdown, and the measurements were carried out under different electric fields, temperatures, frequencies, and cycling conditions. All P–E hysteresis loops were recorded at a

frequency of 50 Hz unless otherwise specified. X-ray photoelectron spectroscopy (XPS) was performed using a PHI 5000 VersaProbe III instrument to analyse cation valence states and oxygen-related defects.

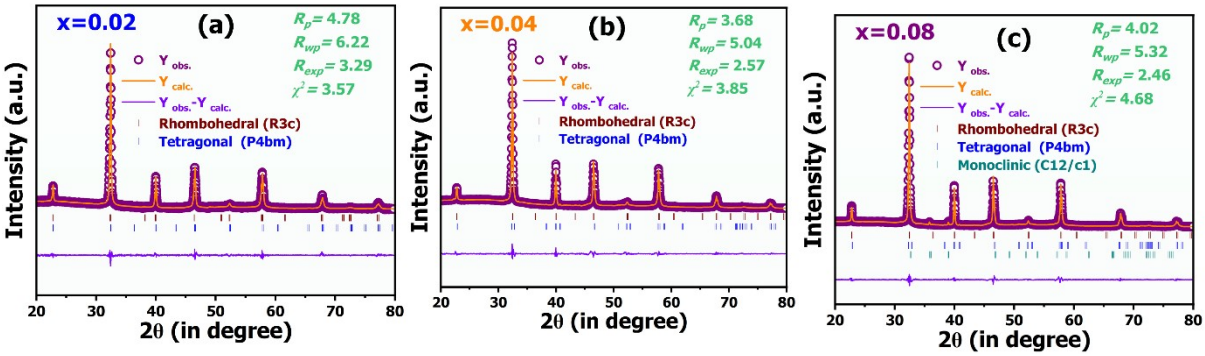

Fig. S1. Rietveld refinement of XRD patterns of x=0.02, 0.04, and 0.08 of (1-x)BNBT-xCCTO.

Table S1. Structural parameters obtained using Rietveld refinement with R3c and P4bm space groups for [(1-x)BNBT-xCCTO] compositions, where x varies as 0.0, 0.02, 0.04, 0.06, and 0.08

[**Symbols:** Rhombohedral with Space Groups **R3c (R),** and tetragonal with Space Group **P4bm (T)**]

SBT Contents (x)	*Phase (%)*		*Lattice constants and cell volume*				R_p	R_{wp}	R_{exp}	χ^2
	Name	%	a	b	c	V				
0.00	R3c	62.08	5.52129	5.52129	13.48526	356.017	4.67	5.87	3.15	3.47
	P4bm	37.92	5.52506	5.52506	3.90434	119.185				
0.02	R3c	31.99	5.52913	5.52913	13.56291	359.084	4.78	6.22	3.29	3.57
	P4bm	68.01	5.52207	5.52207	3.89997	118.923				
0.04	R3c	15.65	5.54102	5.54102	13.30814	353.856	3.68	5.04	2.57	3.85
	P4bm	84.35	5.52388	5.52388	3.90565	119.174				
0.06	R3c	6.04	5.54078	5.54078	13.25752	352.480	3.93	5.23	2.62	3.99
	P4bm	91.62	5.52203	5.52203	3.90188	118.979				
	C 1 2/c 1	2.34	4.68897	3.39154	5.10593	80.075				
0.08	R3c	3.39	5.54166	5.54166	13.25369	352.490	4.02	5.32	2.46	4.68
	P4bm	92.81	5.52173	5.52173	3.90391	119.028				
	C 1 2/c 1	3.80	4.68492	3.40566	5.05141	79.511				

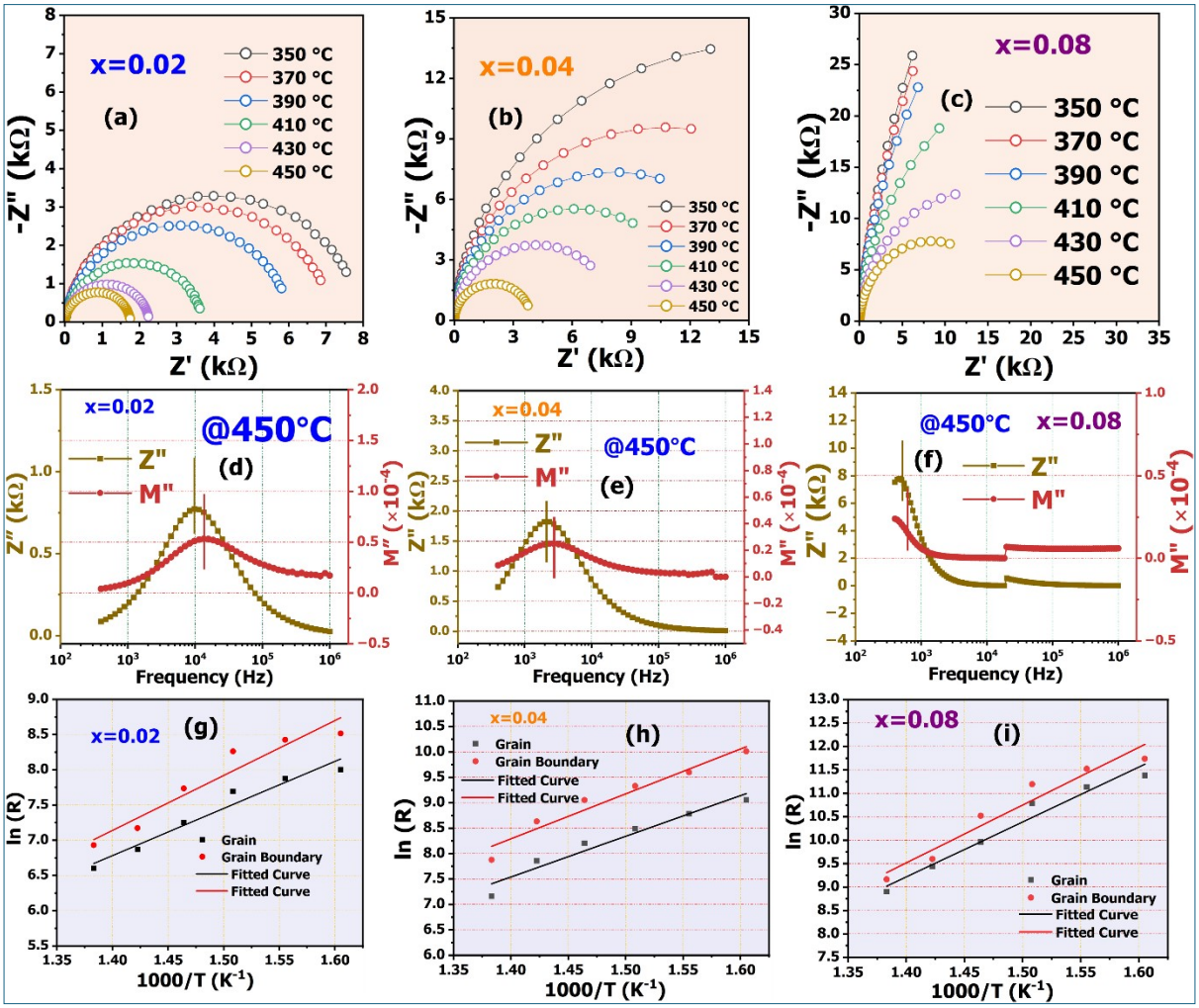

Fig. S3. Electrochemical impedance spectroscopy (EIS) analysis of (1−x)BNBT–xCCTO ceramics with x = 0.02, 0.04, and 0.08. **(a–c)** Nyquist plots recorded at different temperatures (350–450 °C); **(d–f)** frequency dependence of imaginary impedance (Z″) and electric modulus (M″) measured at 450 °C; **(g–i)** Arrhenius plots of grain and grain-boundary resistances extracted from equivalent-circuit fitting.

Table S2. Equivalent circuit fitting parameters R_g and R_{gb} (Ω) for the (1-x)BNBT-xCCTO ceramics.

x↓	Temp.→	350°C	370°C	390°C	410°C	430°C	450°C
0.00	R_g	1911	1537	1312	1053	883	527
	R_{gb}	3637	3169	2478	1669	1291	899
0.02	R_g	2989	2636	2194	1410	963	737
	R_{gb}	4987	4569	3869	2286	1302	1023
0.04	R_g	8562	6527	4863	3654	2584	1287
	R_{gb}	22256	14732	11256	8532	5621	2635
0.06	R_g	30925	23532	17221	10522	5134	3086
	R_{gb}	85287	64852	46624	27321	12521	8022
0.08	R_g	87654	68569	48425	21207	12563	7342
	R_{gb}	125164	100961	72686	37053	14765	9534

Table S3. The calculated tolerance factor (t) values of (1-x)BNBT-xCCTO (R_{Na}^{+} = 1.39 Å, CN=12; R_{Bi}^{3+} = 1.36 Å, CN=12; R_{Ba}^{2+} = 1.61 Å, CN=12; R_{Ca}^{2+} = 1.34 Å, CN=12; R_{Cu}^{2+} = 0.57 Å, CN=4; R_{Ti}^{4+}=0.605Å, CN=6; Ro^{2-}=1.40 Å, CN=6) [1,2].

SBT Contents (x)	Tolerance Factor (t)
0.00	0.98364
0.02	0.97922
0.04	0.9748
0.06	0.97038
0.08	0.96596

For ABO_3 perovskite ceramics, "tolerance factors" (t) are often used to predict the stability of the perovskite structure:

$$t = \frac{R_A + R_O}{\sqrt{2}(R_B + R_O)}$$

Where R_A, R_B, and R_O are the average ionic radii of A cation, B cation, and oxygen anion, respectively [3].

Table S4. A comparison of x=0.06 ceramic with recently reported lead-free energy storage ceramics in terms of W_{rec}, E_b, η, and W_{rec}/E.

Sl. No.	Material type	Composition (testing frequency/electric field waveform)	W_{rec} (J cm^{-3})	E_b (kV cm^{-1})	η (%)	W_{rec}/E_b (mC cm^{-2})	Sample Thickness (μm)	Ref. (year)
	BT-based	0.9(0.7BT-0.3$B_{0.5}SG_{0.3}$F)-0.1BMZ (NA)	4.72	350	85	0.01349	100	[4] (2026)
		0.96BST–0.04BLT (NA)	3.2	400	79	0.00800	NA	[5] (2026)
		0.92(0.7BT-0.3NBT)-0.08SAN (NA)	7.5	670	92.4	0.01119	NA	[6] (2026)
		0.88BTH-0.12BZT (NA)	4.4	500	94	0.00880	100-80	[7] (2025)
		BT-BMT-0.16Ca (NA)	6.74	610	83.05	0.01105	60	[8] (2025)
	NN-based	0.90NN-0.10BLYDTMH (10 Hz / NA)	6.1	610	52.7	0.01000	50-70	[9] (2026)
		0.91NN−0.09CS− (W, Mn) (NA)	5.36	700	75.25	0.00766	60	[10] (2025)
		0.9NN-0.1BNTZ (NA)	3.53	242.2	74.2	0.01457	200 to 30	[11] (2025)
		0.85[0.9NN-0.1LBMT]-0.15CT (NA)	4.02	470	87	0.00855	100	[12] (2025)
		$(Na_{0.94}La_{0.06})(Nb_{0.88}Zr_{0.12})O_3$ (10 Hz / NA)	5.00	710	81.17	0.00704	50	[13] (2025)
	BKT-based	BKT-BST-CT (NA)	5.78	380	87.9	0.01521	NA	[14] (2024)
		BKT-0.5CT (NA)	6.03	500	91.2	0.01206	70-50	[15] (2024)
		0.96(0.6BKT-0.4SBT)-0.04BMF (NA)	4.25	360	87	0.01181	100	[16] (2023)
		BKST50 (1 Hz / Triangular)	2.25	240	73.7	0.00937	200	[17] (2023)
	BNT-based	BNBT-SBT-0.07NN (NA)	7.46	697	82.3	0.01070	50	[18] (2026)
		BNT-SST-0.3NBNM (NA)	5.5	420	79	0.01309	NA	[19] (2026)
		NBBCT-0.05SNA (1 Hz / NA)	2.37	160	88.24	0.01481	NA	[20] (2026)
		0.8[0.94(BNYT-0.06BMT)]-0.2BSTH (NA)	6.14	410	91.32	0.01497	NA	[21] (2025)
		0.85BNT-0.15CTA (NA)	5.89	370	87.4	0.01592	NA	[22] (2025)
		0.40BNT–0.60BZT (100 Hz / NA)	4.1	240	91	0.01708	130-100	[23] (2025)
		BF-BKT-0.4CT	6.24	685	81.4	0.00911	50-40	[24]

		(NA)						(2025)
	BF-based	(0.67BFO-0.33BTO)-SN-0.03 (10 Hz / NA)	6.12	355	80	0.01724	NA	[25] (2025)
		0.8BFBT-0.2NTN (10 Hz / NA)	6.44	440	87	0.01464	100	[26] (2025)
		0.67BFO-0.33BTO-0.09SNMAZZ (NA)	5.31	315	76.9	0.01686	80-50	[27] (2025)
		BFST-0.05NN (10 Hz / NA)	4.98	340	67	0.01465	NA	[28] (2025)
	KNN-based	0.85KNN-BCZT-0.15NBST (NA)	7.48	500	75.06	0.01496	200-100	[29] (2025)
		KNLN-0.15SZ (NA)	4.06	400	75	0.01015	100	[30] (2025)
		KNN–0.08BCMS (NA)	5.8	360	83.5	0.01611	100	[31] (2025)
		0.94KLNN-0.06CMT (10 Hz / NA)	6.4	370	73.6	0.01730	100	[32] (2025)
		KNN-0.15 (NA)	6.36	580	84	0.01096	60-50	[33] (2025)
	SBT-based	SBT-0.15BNiT (NA)	5.12	460	97.13	0.01113	70-50	[34] (2026)
		0.62SBT-0.38KBT-1%LNS (10 Hz / NA)	4.07	230	79.75	0.01769	200	[35] (2025)
		$Sr_{0.7}Bi_{0.15}Ho_{0.05}TiO_3$ (NA)	2.16	300	95.8	0.00720	NA	[36] (2024)
		$Sr_{0.6}(Li_{0.5}La_{0.5})_{0.1}Bi_{0.2}TiO_3$ (NA)	4.4	420	90	0.01048	NA	[37] (2024)
		SBT-0.15BCT (NA)	2.31	238	82	0.00970	150-100	[38] (2024)
	AN-based	ABCN1 (1 Hz / NA)	4.4	205	63	0.02146	210-170	[39] (2025)
		$Ag_{0.94}Yb_{0.02}NbO_3$ (10 Hz / NA)	4.05	270	61	0.01500	NA	[40] (2025)
		ALS5N (10 Hz / NA)	4.32	315	51.39	0.01371	100	[41] (2025)
		ASNN0.05 (NA)	3.9	300	83	0.01300	200-100	[42] (2025)
		AMN-1.5Sm (10 Hz / NA)	5.18	320	73.3	0.01619	100	[43] (2025)
	This work	0.94BNBT-0.06CCTO (50 Hz / Triangular)	4.69	202	90.47	**0.02322**	200 to 100	**This Work**

[NA: Data not reported in original publication]

["NA: Thickness not available in reference; comparison made based on reported electric field strength and W_{rec}."]

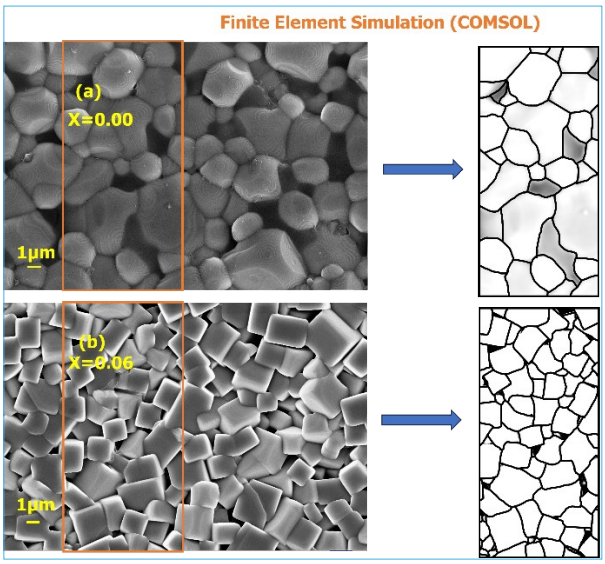

Figure S4. FESEM-derived microstructural input used for finite-element simulations. Representative cropped regions from the main FESEM images of (a) x = 0.00 and (b) x = 0.06 ceramics, showing the extracted grain boundaries employed to construct the two-dimensional COMSOL simulation domains.

References:

1 R. D. Shannon, *Acta Cryst.*, 1976, A**32**, 751–767.

2 H. Qi, R. Zuo, J. feng Li and L. Li, *J. Eur. Ceram. Soc.*, 2018, **38**, 5341–5347.

3 Y. Ning, Y. Pu, X. Zhang, Z. Chen, C. Wu, L. Zhang, B. Wang and X. Li, *Mater. Today Phys.*, 2024, **43**, 101418.

4 S. Zhang, L. Yang, X. Miao, R. Jing, Z. Deng, J. Luo, Y. Zhang, A. Zhang and M. Zeng, *J. Eur. Ceram. Soc.*, 2026, **46**, 117916.

5 B. Zhang, Y. Gu, K. Ma, D. Wang, X. Zhang and X. Qi, *J. Energy Storage*, 2026, **141**, 119222.

6 D. Ballo, S. Wang, J. Qian, G. Ge, Y. Liu, Z. Mu and J. Zhai, *Ceram. Int.*, 2026, **52**, 8706-8716.

7 T. Li, J. Yin and J. He, *Ceram. Int.*, 2025, **51**, 57800–57806.

8 H. Qi, S. Yan, B. He, M. Xie and G. Wang, *J. Mater. Sci. Mater. Electron.*, 2025, **36**, 1471.

9 S. Zou, W. Fan, L. Tong, Y. Gu, X. Zhang and X. Qi, *J. Mater. Chem. A*, 2026, **14**, 2497–2506.

10 B. Liu, M. Wang, X. Wang, L. Chen, Q. Zhao, Q. Mi, M. Chu, T. Wang, J. Ding and Y. Li, *Ceram. Int.*, 2025, **51**, 57238–57248.

11 X. Zhong, A. Shui, H. Yu and Y. Fang, *J. Alloys Compd.*, 2025, **1010**, 177559.

12 H. Wen, X. Wu, N. Zhou, H. Li and J. Cao, *J. Mater. Sci. Mater. Electron.*, 2025, **36**, 1–15.

13 X. Zhai, M. Lu, J. Du, J. Hao, W. Kuai, Z. Gai, M. Zhao and L. Zheng, *J. Eur. Ceram. Soc.*, 2025,

45, 117151.

14 P. Zheng, L. Sheng, W. Wang, Y. Ying, K. Zhang and J. Wang, *ACS Appl. Electron. Mater.*, 2024, **6**, 6932–6939.

15 X. Li, J. Xi, C. Li, W. Bai, S. Wu, P. Zheng, P. Li and J. Zhai, *J. Mater. Chem. A*, 2024, **12**, 32359–32370.

16 R. Kang, Z. Wang, Y. Zhao, Y. Li, Y. Hu, X. Hao, L. Zhang and X. Lou, *J. Alloys Compd.*, 2023, **935**, 167999.

17 M. Kitamura, S. Fujihara and M. Hagiwara, *J. Eur. Ceram. Soc.*, 2023, **43**, 6069–6076.

18 X. Lei, F. Zhang, M. Li, J. Liu, X. Ma, C. Wang, X. Gao and Z. J. Wang, *J. Energy Storage*, 2026, **141**, 119557.

19 H. Lian, S. Lv, W. Gao, M. Shi and X. Chen, *J. Mater. Sci. Mater. Electron.*, 2026, **37**, 118.

20 Z. Li, X. Zhao, J. Zhang and J. Zhang, *Mater. Sci. Eng. B*, 2026, **323**, 118712.

21 X. Zeng, Y. Zhang, J. Shen, X. Jiang, S. Wang, H. Dai, X. Wu, M. Gao, C. Zhao, T. Lin, L. Luo, J. Lin, B. Sa and C. Lin, *Small*, 2025, **21**, 2406080.

22 J. Fan, L. Wang, J. Wang, Z. Cheng, L. Zhong, T. Yang and Z. Hu, *Inorg. Chem. Front.*, 2025, **12**, 1444–1454.

23 W. Zhou, Y. Zhang, Y. Zhang, X. Yang, X. Zhang, Q. Zhang, S. Jiang, G. Zhang, Y. Chen and M. Shen, *J. Am. Ceram. Soc.*, 2025, **108**, e20382.

24 W. Zhang, S. Chen, J. Lv, J. Hu, T. Wang, H. Luo, J. Liu, W. Gong and Z. Pan, *Ceram. Int.*, 2025, **51**, 51299–51306.

25 J. Zhang, Y. Pu, Y. Hao, Q. Pan, Y. Han, Y. Yang, L. Zhang and B. Wang, *Chem. Eng. J.*, 2025, **516**, 164008.

26 C. Peng, A. Shui, H. Yu and X. Zhong, *Ceram. Int.*, 2025, **51**, 52741–52750.

27 Y. Pu, J. Zhang, Y. Hao, Y. Yang, P. Lv, L. Zhang, B. Wang and Y. Wang, *J. Alloys Compd.*, 2025, **1040**, 183487.

28 J. Zhang, Y. Pu, Y. Hao, B. Wang, Y. Han, Y. Yang and L. Zhang, *J. Eur. Ceram. Soc.*, 2026, **46**, 117920.

29 L. Diwu and Z. Sun, *Ceram. Int.*, 2025, **51**, 51672–51678.

30 Y. Yang, Z. Liu, L. Gao, Z. Wang, K. Guo, P. Mao, B. Xie, Y. Tian, F. Xue and L. Shu, *ACS Appl. Mater. Interfaces*, 2025, **17**, 22963–22973.

31 L. Zhang, X. Zhu, J. Yin, W. Li, X. Tang, R. Zhao, K. Chen, Z. Jian, Y. Zhao, Y. Liu, Y. Jiang, X. Guo and K. Yan, *Ceram. Int.*, 2025, **51**, 65264–65272.

32 X. Zhang, S. Dang, Y. Wang, Q. Chai, Z. Peng, D. Wu, P. Liang, L. Wei, X. Chao and Z. Yang, *Small*, 2025, **21**, e08980.

33 Y. Tao, H. Yang, M. Wang, B. Zheng and Y. Lin, *J. Alloys Compd.*, 2025, **1024**, 180210.

34 Y. Mao, J. Zhang, M. Chen, M. Fang, N. Yan, Z. Lou and Y. Zhou, *Scr. Mater.*, 2026, **273**, 117101.

35 H. Zheng, Y. Gu, K. Ma, X. Zhang and X. Qi, *J. Energy Storage*, 2025, **112**, 115550.

36 J. Chen, P. Zhao, F. Si, Y. Li, S. Zhang, Z. Fang and B. Tang, *Ceram. Int.*, 2024, **50**, 13208–13218.

37 J. Chen, P. Zhao, K. Chen, F. Si, Z. Fang, S. Zhang and B. Tang, *Chem. Eng. J.*, 2024, **502**, 157866.

38 R. Chen, Y. Wang, W. Zhao, Y. Chen, L. Zhao and B. Cui, *J. Mater. Sci. Mater. Electron.*, 2024, **35**, 916.

39 Z. Yan, J. He, H. Chen, D. Zhang, Y. Liu, H. Luo, C. Li, I. Abrahams and H. Yan, *Small*, 2025, **21**, 2500810.

40 Z. Lin, W. He, Y. Liu, C. Luo, A. You, W. Chao, J. Chen, J. Li, M. Chen and X. Wang, *ACS Appl. Eng. Mater.*, 2025, **3**, 3127–3135.

41 M. Chu, P. An, H. Yang, C. Cai and Q. Mi, *J. Mater. Sci. Mater. Electron.*, 2025, **36**, 1085.

42 Y. Tian, S. Guo, Y. Jia, T. Xia, Y. Xu, L. She, Z. Sun, Y. Wu, W. Ge, L. Jin and X. Wei, *J. Eur. Ceram. Soc.*, 2025, **45**, 117481.

43 B. Yang, W. Xu, Y. Zhang, Z. Xu, S. Wu, X. Wu, C. Zhao, T. Lin, M. Gao and C. Lin, *J. Eur. Ceram. Soc.*, 2025, **45**, 117218.